MDPI

Biocomposite Films of Amylose Reinforced with Polylactic Acid by Solvent Casting Method Using a Pickering Emulsion Approach

Marwa Faisal [1], Jacob Judas Kain Kirkensgaard [2,3], Bodil Jørgensen [1], Peter Ulvskov [1], Max Rée [1], Sue Kang [1], Nikolai Andersson [1], Mikkel Jørgensen [1], Jonas Simonsen [1], Kim H. Hebelstrup [4,5] and Andreas Blennow [1,*]

[1] Department of Plant and Environmental Sciences, Faculty of Science, University of Copenhagen, 1871 Frederiksberg C, Denmark; marwa@plen.ku.dk (M.F.); boj@plen.ku.dk (B.J.); ulvskov@plen.ku.dk (P.U.); jcv708@alumni.ku.dk (M.R.); nzx474@alumni.ku.dk (S.K.); mtj503@alumni.ku.dk (N.A.); nck558@alumni.ku.dk (M.J.); tgx739@alumni.ku.dk (J.S.)
[2] Department of Food Science, Faculty of Science, University of Copenhagen, 1958 Frederiksberg C, Denmark; jjkk@food.ku.dk
[3] Niels Bohr Institute, Faculty of Science, Universitetsparken 5, 2100 København Ø, Denmark
[4] Department of Agroecology, Aarhus University, 4200 Slagelse, Denmark; kh@plantcarb.com
[5] PlantCarb ApS, 2970 Hørsholm, Denmark
*   Correspondence: abl@plen.ku.dk

Abstract: Binary and ternary blends of amylose (AM), polylactic acid (PLA), and glycerol were prepared using a Pickering emulsion approach. Various formulations of AM/PLA with low PLA contents ranging from 3% to 12% were mixed with AM matrix and reinforced with 25% cellulose nanofibers (CNF), and PLA-grafted cellulose nanofibers (g-CNF), the latter to enhance miscibility. Polymeric films were fabricated through solvent casting and characterized using Scanning Electron Microscopy (SEM), Fourier Transform Infrared Spectroscopy (FTIR), and Wide-Angle X-ray Scattering (WAXS), and the evaluations of physical, mechanical properties, and wettability were performed using contact angle measurements. The binary blends of AM and PLA produced films suitable for packaging, pharmaceutical, or biomedical applications with excellent water barrier properties. The ternary blends of AM/CNF/PLA and AM/g-CNF/PLA nanocomposite films demonstrated enhanced tensile strength and reduced water permeability compared to AM/PLA films. Adding g-CNF resulted in better homogeneity and increased relative crystallinity from 33% to 35% compared to unmodified CNF. The application of Pickering emulsion in creating AM-based CNF/PLA composites resulted in a notable enhancement in tensile strength by 47%. This study presents an effective approach for producing biodegradable and reinforced PLA-based nanocomposite films, which show promise as bio-nanocomposite materials for food packaging applications.

Keywords: biocomposites; Pickering emulsion; starch; amylose; cellulose nanofibers; polylactic acid

1. Introduction

The utilization of petroleum-based plastics in food packaging poses significant environmental challenges due to their slow decomposition, contributing to the accumulation of plastic waste that can harm natural ecosystems. This issue underscores the imperative for alternatives to reduce plastic waste in food packaging. Additionally, global concerns about the health impacts of plastics stem from leaching compounds, further emphasizing the need for a sustainable approach to packaging materials [1].

The emergence of bioplastics, derived from renewable sources, offers a viable solution to address the environmental issues associated with traditional plastics. Various materials and techniques have been successfully employed to manufacture bioplastics, utilizing natural polymers such as amylose, starch, proteins, and cellulose. Notably, starch and cellulose, due to their abundance in nature, are extensively utilized in bioplastic production [2]. Both

are polysaccharides and their hydrophilic nature poses a compatibility challenge when used in composites with most known matrices, as these are substantially less hydrophilic.

Starch comprises two biopolymers, namely amylose (AM) and amylopectin. AM is a mainly linear polymer composed of α-(1,4)-linked glucose units, predominantly contributing to the amorphous phase [3]. In contrast, amylopectin has an α-(1,4)-linked glucan backbone featuring α-(1,6)-linked side-chains. The stable double-helical junction zones observed in starch are attributed to amylopectin and the amylopectin content of conventional high-amylose starches poses challenges for biomaterial applications [4]. Our unique capability to produce virtually pure (99%) AM in bulk quantities in transgenic barley grains at a reasonable cost has overcome previous challenges associated with the costly separation of AM from amylopectin, providing an enabling resource for biocomposites [5,6].

Utilizing conventional starch as a raw material for bioplastics presents drawbacks, including high hydrophilicity and brittleness. Our prior investigations have demonstrated that utilizing pure AM can significantly increase the mechanical strength compared to regular starch. Furthermore, AM exhibits high gelatinization temperature, providing thermal stability comparable to semi-natural bioplastics like MaterBi® [7]. Numerous studies have been devoted to comprehending the properties of starch in biocomposites, particularly those involving polylactic acid (PLA) [8].

PLA has garnered attention within the biopolymers family due to its high strength and modulus in comparison to petroleum-based polymers like polyethylene terephthalate (PET). PLA finds applications in high-value medical uses, including implant devices. However, PLA faces limitations arising from its suboptimal barrier properties and limited thermal stability [9]. Crystallinity is also a desirable parameter. Pure PLA has a higher amorphous phase compared to the crystalline phase, which facilitates gas permeability [10]. PLA is not very flexible and fails at quite moderate deformations. Consequently, various approaches have been proposed to improve its properties, including the blending of PLA with other materials as a straightforward and cost-effective strategy to address shortcomings, such as the incorporation of silicates and 1, 3, 5-benzene tricarboxyamide (BTA) [11,12]. The physical properties of PLA-layered silicate nanocomposites are sensitive to large-scale chain movements; silicates restrict the mobility of the surrounding polymer chains. The effect could be improved via compatibilization using modifiers [11].

Another approach for reducing the rigidity of PLA-based materials consists of its plasticization that can be achieved simply through blending the PLA matrix with low molecular weight additives or another miscible polymer. A series of 1, 3, 5-trialkyl-benzenetricarboxylamides (BTA-Rs) with different side-chain lengths of n-alkyl are synthesized to use as nucleating agents of poly (lactic acid) (PLA). It is found that 0.8 wt.% is the optimal weight fraction of BTA-nBu to improve the crystallization of PLA; the nucleation efficiency can reach up to 91% with no effect of crystalline structure [12].

However, those fillers are generally not recyclable and not biodegradable. Replacing these with natural polymers like amylose is challenging due to the limited compatibility between the hydrophilic amylose and the hydrophobic thermoplastic matrix, which results in poor dispersion [13].

The incorporation of PLA into starch composites enhances both the mechanical strength and hydrophilicity of the resulting bioplastics. Investigations on cornstarch and PLA biocomposites aim to discern the interaction and miscibility of PLA and starch with glycerol. However, exceeding a PLA concentration of 10% can affect the production costs of bioplastics on an industrial scale [14]. A previous study [15] successfully extruded starch-based PLA with lower concentrations (3, and 10%) at 90–150 °C and compression molding at 150 °C. The study showed a low density of starch-based PLA and better mechanical and barrier properties for developing food packaging biocomposites at 10% of PLA.

The primary challenge in achieving a blend based on starch and PLA with desirable properties lies in enhancing the interfacial adhesion between hydrophilic starch molecular segments and hydrophobic PLA phases, leading to suboptimal dispersion. Chemical modifications to starch, such as etherification, increase the compatibility with PLA more

than other treatments of starches, which contain a high amount of amylose [16]. Numerous efforts have been undertaken to enhance compatibility in starch/PLA blends through the incorporation of compatibilizers. Binary blends have been investigated with compatibilizers, such as PLA-g-MA and a maleic anhydride-grafted polyethylene glycol-grafted starch (mPEG-g-St) [17–19]. The outcome of these trials indicates a positive deviation in the tensile properties of the blend samples, with no discernible impact on biodegradability behavior, underscoring the effectiveness of the compatibilizer.

Blending AM with other polysaccharides offers an avenue for improving barrier properties, mechanical strength, and thermal stability, especially when combined with cellulose nanofibers (CNF) [20]. Blending CNF into AM has demonstrated improvements in various properties due to the interaction of α- and β-glycosidic polysaccharides. CNF can be sourced from various agricultural wastes, primarily composed of the primary cell wall, offering a simpler and cleaner extraction method compared to using wood as a raw material. The successful extraction of CNF from sugar beet involves alkaline treatment to remove non-cellulosic components, the oxidation of phenolic compounds, and subsequent high-shear homogenization [21]. Previous research has indicated that AM-CNF composites exhibit superior mechanical properties, reduced permeability, and lower contact angles compared to the individual materials [20].

The abundant hydroxyl groups on polysaccharide surfaces, such as CNF, enable grafting with other functional groups onto the surface, offering a strategy to enhance the cellulose/thermoplastic interface. A common grafting method involves a "grafting from" approach, wherein a covalent bond is formed between the polysaccharide and the polymer. A well-known process involves the polymerization of L-lactide in the presence of, e.g., cellulose, resulting in PLA oligomers grafted onto the cellulose surface [22]. This process can be accomplished either in a solvothermal state or through polymerizing L-lactide in a molten state in the presence of the polymer [23,24]. It is important to note that, due to the thermal degradation of CNF at high temperatures, challenges persist in using melt processing and injection molding, necessitating the careful selection of the matrix material [25,26].

In this study, CNF serves as an emulsion stabilizer by adsorbing onto the interface between the two immiscible phases. The application of Pickering emulsion in creating PLA-based TEMPO-oxidized bacterial cellulose composites resulted in a notable enhancement in bending strength and tensile strength. The even distribution of the TEMPO-oxidized bacterial cellulose within the PLA matrix aids in establishing a three-dimensional network and cross-linking arrangement. This network serves as a nucleating agent, facilitating the crystallization of PLA [27–29].

Binary and ternary blends, consisting of AM, PLA, CNF, and g-CNF, were prepared using the Pickering emulsion approach and dried at 50 °C. Given the limited exploration of lower concentrations of AM and PLA, our objective is to investigate a bioplastic blend based on PLA and AM using the Pickering emulsion approach with low percentages of PLA (0, 3, 6, and 12%). Few studies have examined the integration of starch-based bioplastics with minimal amounts of PLA. Our objective is to develop highly compostable blends of PLA and AM-based bioplastic, utilizing low PLA concentrations (0, 3, 6 and 12%) to regulate the biodegradation process of polysaccharides. Through our approach of using grafted starch, compatibility between starch and PLA was enhanced, requiring less CNF and g-CNF being incorporated into the bioplastic composites, and the produced materials were characterized by physical, mechanical, hydrophobicity, and morphological observations. The overarching goal of this research is to use pure, bulk AM to develop a novel ternary blend of AM/CNF/PLA and AM/g-CNF/PLA using a Pickering emulsion solvo-casting method. Film properties were assessed after drying at moderate temperatures, eliminating the need for heat-intensive processing methods.

2. Materials and Methods

2.1. Materials

AM (99%) granules were extracted from a transgenic barley generated using starch branching enzyme RNA interference as described in [6]. The extracted product contained 90% starch and 10% impurities, whereas 99% of the starch consists of AM. PLA product Global Pond Cycle® code "IMF105" was provided by Pond Global (Århus, Denmark). Glycerol, dichloromethane (DCM), and toluene (anhydrous, 99.8%) were all obtained from Sigma-Aldrich. Both dried and wet CNF (85%) derived from sugar beet pulps were kindly provided by Nordic Sugar A/S. L-lactide, and Tin (II) ethylhexanoate (Sn (Oct)$_2$) (95%, Aldrich, St. Louis, MO, USA) was purchased from Sigma and used as received without further purification.

2.2. Methods

2.2.1. CNF Grafting

The grafting of CNF fibers was attained through in situ ring polymerization, as detailed in previous studies [22,26]. Initially, 5 g of dry CNF was dispersed in toluene at 80 °C and continuously stirred under a nitrogen flow to evaporate the toluene. Subsequently, L-lactide monomer (20 g) was dissolved in hot toluene and introduced into the reaction flask. Upon thorough mixing, the catalyst Sn (Oct)$_2$ (2 wt.% by lactide weight) was added, and the reaction proceeded for 24 h under a nitrogen atmosphere. Following cooling, the resulting material was filtered, and the solid portion was washed three times with DCM and ethanol to eliminate any ungrafted PLA and residual L-lactide.

2.2.2. Characterization of Grafted CNF

Upon completion of the 24 h reaction period, the reaction flask was cooled, and the CNF solution was precipitated in 500 mL of cold methanol, resulting in a white solid. The precipitate was centrifuged and washed with 500 mL methanol three times, followed by rinsing with ethanol thrice to remove any residual L-lactide. After overnight drying at room temperature to remove solvent traces, the material was further dried in a vacuum oven at 60 °C until complete desiccation. The conversion degree of the monomer was determined using a gravimetric method [22,30] according to Equation (1):

$$C_g = (A - B/D) \times 100$$

where C_g is the conversion degree, A is the total mass produced after polymerization, B is the mass of the CNF, and D is the L-lactide monomer mass used in the reaction.

The solid obtained was dissolved in 200 mL of DCM to obtain the modified CNF for ensuing analysis. This procedure involved dissolving the solid and separating the resulting solution through centrifugation, with two additional steps of purification using DCM. The polymerized L-lactide (PLLA) extracted from this process was once again precipitated in methanol for further analysis. The grafting yield was then calculated using Equation (2):

$$\text{Grafted yield} = ((m_{\text{g-CNF}} - m_{\text{CNF}})/m_{\text{CNF}}) \times 100$$

where $m_{\text{g-CNF}}$ is the mass of the g-CNF produced in grams after washing with DCM and drying, and m_{CNF} is the mass of original CNF in grams.

The obtained grafted fibers, termed g-CNF (the fibers produced according to Section 2.2.1), were characterized using infrared spectroscopy (FTIR and WAXS (according to Sections Fourier Transform Infra-Red (FT-IR) Spectroscopy and Wide-Angle X-ray Scattering (WAXS))).

2.2.3. Blends Preparation Using a Pickering Emulsion Approach

An AM film was obtained by adding 30 wt.% glycerol to a 3% AM suspension and heated in a glass reactor at 140 °C for 30 min in a high-pressure glass reactor. The solutions were cooled to 70 °C then cast in Teflon-coated Petri dishes. The films were dried at 35 °C

in ventilated oven until complete dryness. Glycerol wt.% was fixed in all composites based on our previous work to avoid brittle matrices [20].

For the binary AM/PLA blend, AM was suspended in water and mixed with a 10% (wt/v) solution of PLA in DCM. The ratio of water to DCM was 5:1 (*v*/*v*) (250 mL of AM in water: 50 mL of PLA in DCM). The mixture was then sonicated for 15 min using a 500 W QSonica with a 25.4 mm horn. A control sample of AM was produced using the same procedure and concentration. After sonication, the resulting slurry of AM/PLA micro-particles was stirred and left in a fume hood overnight to evaporate the DCM. Once the solvent volume was evaporated, the mixture was poured into Petri dishes and left to dry overnight at 50 °C.

For the binary blend, PLA was added to the AM matrix at ratios of 3%, 6%, and 12% by weight. For the ternary blend, CNF aqueous suspension and dry g-CNF content was based on 25% by weight of AM and added to the binary AM/PLA suspensions. Pure AM was considered as a control sample, and the total mass percentage of the sample was 100%. The composition and codes of the samples are depicted in Table 1.

Table 1. Formulations of AM/PLA composites and corresponding mass of AM/PLA, AM/PLA/CNF and AM/PLA/-g-CNF used.

Code	AM (wt.%)	PLA (wt.%)	Glycerol (wt.%)	CNF (wt.%)	g-CNF (wt.%)
AM/PLA blends					
AM	77	0	23	0	0
AM/3PLA	67	3	23	0	0
AM/6PLA	64	6	23	0	0
AM/12PLA	58	12	23	0	0
AM/CNF/PLA blends					
AM/CNF/3PLA	59	3	23	15	0
AM/CNF/6PLA	57	6	23	14	0
AM/CNF/12PLA	52	12	23	13	0
AM/g-CNF/PLA blends					
AM/g- CNF/3PLA	59	3	23	0	15
AM/g- CNF/6PLA	57	6	23	0	14
AM/g-CNF/12PLA	52	12	23	0	13

2.2.4. Films Production and Characterization

Fourier Transform Infra-Red (FT-IR) Spectroscopy

FT-IR spectra of the film samples were recorded on a Bomem MB100 FTIR spectrometer (ABB-Bomem, Quebec, QC, Canada), using an attenuated total reflectance (ATR) single reflectance cell with a diamond crystal. The samples were scanned 64 times over the range of 4000–600 cm^{-1} at a resolution of 4 cm^{-1} against air as the background. The FTIR spectra were used to identify chemical interactions between the matrices and natural fillers. Each sample was scanned twice, observing good reproducibility [31].

Wide-Angle X-ray Scattering (WAXS)

WAXS analysis of the film was conducted on a Nano-inXider instrument from Xenocs (Grenoble, France) using a Cu Kα source with a 1.54 Å wavelength and a 2D 100 K Pilatus detector (Dectris Ltd., Baden, Switzerland). Samples were loaded between mica windows and background contributions were subtracted from the measured spectra. The total relative crystallinity was calculated as the ratio of the crystalline peak area to the total diffraction area using Peak Fit software (Version 4.0. Systat Software Inc., San Jose, CA, USA).

Moisture Content

The water content of the films was determined according to [32]. Using a gravimetric protocol, film samples (2 × 2 cm) were dried in an oven at 105 °C for 24 h. The moisture content of the films was calculated (Equation (1)):

$$MC\% = \left(\frac{Mi - Mf}{Mi}\right) \times 100 \tag{1}$$

Swelling and Water Solubility

The swelling index (SI) and water solubility (WS) were measured gravimetrically using square-shaped pieces of 2 × 2 cm in triplicate [33]. The first mass (M_1) was measured after the samples were kept in an oven for 24 h at 70 °C to reach a constant mass. Afterward, to obtain M_2, each sample was immersed in 20 mL of deionized water and stirred for 24 h at 30 °C. The samples were dried with filter paper and weighed to obtain the wet weight (M_2) of the samples. Lastly, the samples were dried once more at 70 °C for 24 h and measured until a constant weight to obtain M_3.

SI and WS (%) were calculated (2) and (3):

$$SI(\%) = (M2 - M1)/M1 \times 100 \tag{2}$$

$$WS(\%) = (M1 - M3)/M1 \times 100 \tag{3}$$

Mechanical Properties

The films were cut into 4 mm wide and 50 mm long rectangular strips. An Instron instrument model 5569 (MTS, Eden Prairie, MN, USA) equipped with a 5 kN tensile load cell was used to measure tensile properties. The distance between clamps was 60 mm and the crosshead speed was set at 10 mm min^{-1}. For each film, 5–7 samples were measured and averaged. Thickness was measured using a micrometer screw gauge [21].

Scanning Electron Microscopy (SEM)

SEM images were acquired with a Quanta 3D FEG (FEI Company, Eindhoven, The Netherlands) and the surface and cross-sections were acquired. The films were cut into small pieces and attached to a metal plate. Prior to analysis, they were coated with a 2 nm colloidal gold layer. To observe the dispersion of PLA, CNF and g-CNF in the AM matrix in cross-sections, samples were cryogenically fractured in liquid nitrogen and sputtered with gold [20].

Wettability by Contact Angle

The wettability of binary and ternary AM blends was evaluated via the sessile drop contact angle method using distilled water drops of 25 μL at room temperature using a goniometer Model OCA 25 (Data Physics Instrument GmbH, Filderstadt, Germany); samples performed in triplicate [34].

Statistical Analysis

One-way analysis of variance (ANOVA) was applied for the data analysis. Means were compared according to Tukey's test at a significance level of 95% ($p < 0.05$). Statistical analyses were performed using the IBM® SPSS® Statistics 27 software, New York, USA.

3. Results

3.1. Grafting of CNF Align Margins the Same Everywhere, See Below for Example

The synthesis of grafted CNF (g-CNF) involved the ring-opening polymerization (ROP) of PLA from the hydroxyl groups present on the surface of CNF. This technique yields a stable grafted material on the cellulose nanofiber surface, enhancing compatibility with the PLA matrix. The monomer conversion degree and grafting yield, calculated as per

Equations (1) and (2), were found to be 88% and 27%, respectively. The monomer conversion degree aligns with similar studies employing a solvothermal reaction approach [26,35]. The produced g-CNF was analyzed using FTIR and WAXS after washing with DCM, confirming that PLLA(poly L-lactic acid) had been successfully grafted on CNF surface (Figures S1 and S2).

3.2. FTIR of the Composite Films Align Margins the Same Everywhere

This analysis provides a spectrum of bands that are related to various functional groups to identify the materials and to test physical interactions or new chemical bonds. The FTIR spectra showed O–H stretching between 3600 and 3200 cm^{-1} due to the O–H–bonding between glycerol and AM (Figure 1a). The C–H was observed at 2932 cm^{-1} and the absorption band at 1653 cm^{-1} attributed to the water adsorption, due to the hygroscopic nature of polysaccharides [36,37]. The peaks at 1050 to 950 cm^{-1} are attributed to the presence of C–O–C stretching. The PLA spectrum had an intense peak at 1746 cm^{-1}, which corresponds to the C=O stretching of the polyester; in addition, characteristic stretching signals from –CH group can be observed at 2991 cm^{-1} and 2931 cm^{-1} (Figure 1a) [38].
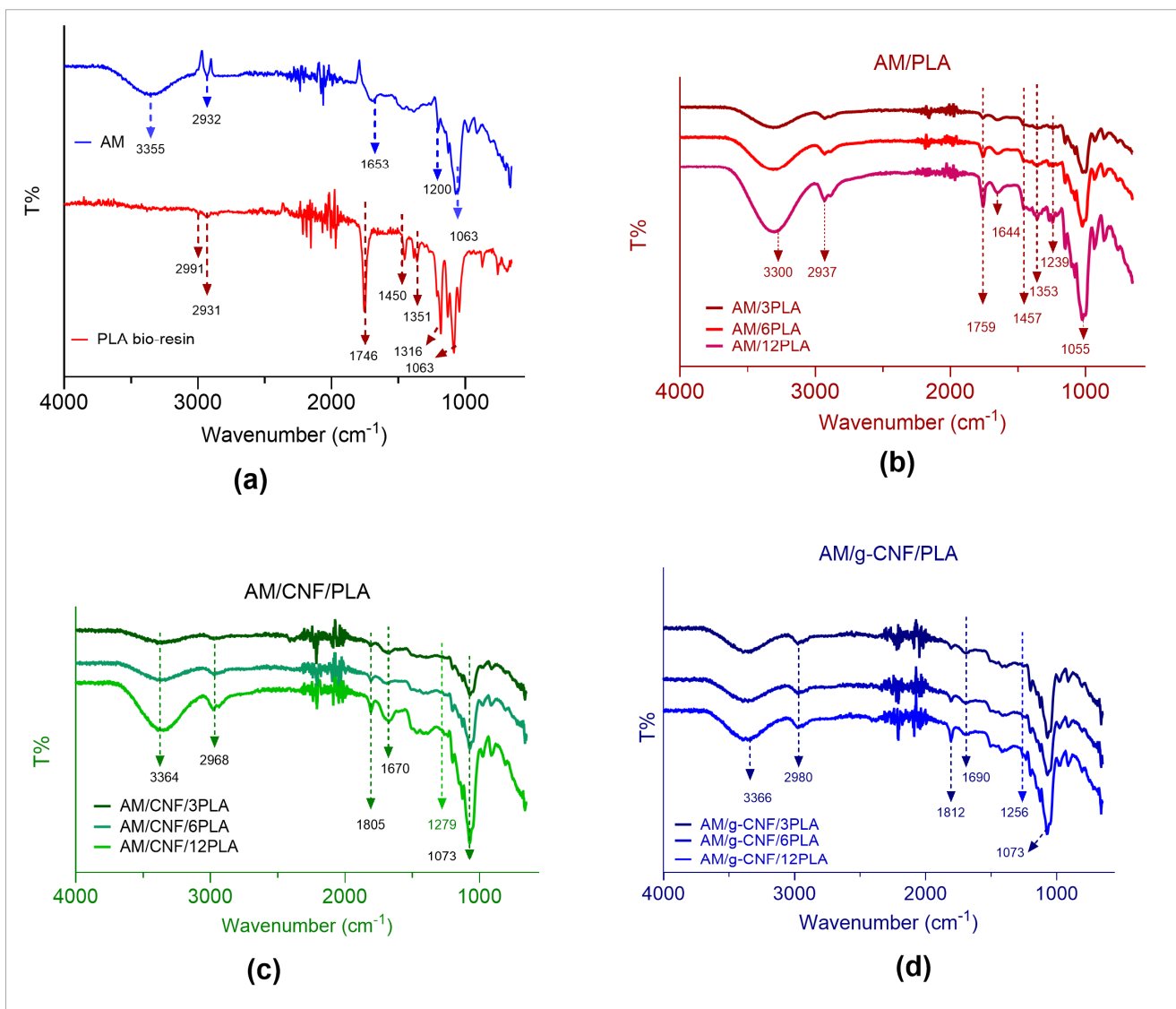
Figure 1. FTIR of (**a**) AM, PLA bioresin, (**b**) composite films of AM/PLA, (**c**) AM/CNF/PLA, (**d**) AM/g−CNF/PLA.

The spectra associated with the AM-PLA films exhibited AM peaks around 3600–3000 cm^{-1} and 1200–980 cm^{-1} (Figure 1b). The intensity of the peak at 1759 cm^{-1}, corresponding to the stretching vibration of carbonyl ester C=O, increased with higher PLA concentrations, while the peaks around 3600–3000 cm^{-1} decreased as PLA content increased, attributable to the lower content of –OH in PLA. The stretching vibration associated with the ester bonds C–O of PLA at 1200 cm^{-1} and 1063 cm^{-1} exhibited an additive effect on the curve, resulting in higher peaks around 1200–980 cm^{-1} (Figure 1a).

Peak shifting indicates a weak inter- and intramolecular hydrogen bond between AM chains. These results showed that PLA hindered the hydrogen bonds of AM molecules (Figure 1b). Nevertheless, it is not sufficient to validate the miscibility of PLA and AM. The same results confirmed that some functional groups were not strong enough to make changes in typical vibration in the composite of PLA and starch-based bioplastics [15]. With the addition of CNF, the peaks seem to shift to higher wavenumbers that can been seen in all AM/PLA/CNF composites (Figure 1c). Similar results were observed with AM/CNF composite films, attributed to the similarities in the polysaccharide chains [20]. Similarly, the grafted AM/PLA/g-CNF films showed a higher wavenumber shift compared to all composite films, albeit with a lower intensity of the –OH peak compared to AM/PLA/CNF (Figure 1d). All the composites have predominant functional groups of hydroxyl groups, whereas composites with 12% PLA have the highest carbonyl groups (Figure 1).

3.3. Crystallinity

The WAXS analysis of the AM film revealed distinct peaks at around 7.6°, 12.6°, and 20°, with smaller peaks observed around 5°, 16.5°, 22.7°, and 23.6° (Figure 2a), corresponding to peaks from the Vh and B crystalline structures, respectively. In the PLA sample, there were two small peaks at 2θ = 12°, 14.5°, and at 22°, which were attributed to the (010), (110/200) and (015) planes, respectively (Figure 2a). In addition, two strong diffraction peaks appear at 2θ = 17° and 19.5°, which ascribed to the (110/200) and (203/113) planes, respectively [10].

The WAXS diffraction patterns of the AM/PLA composite films exhibited peaks at around 7.6°, 12.6°, and 20°, corresponding to the Vh crystalline structure of AM, along with a peak at 17.4° attributed to the pseudo orthorhombic α- crystalline structure of PLA [13]. Notably, the intensity of the peak around 17.4° was relatively weak for 3% PLA, but a prominent increase was observed with higher PLA concentrations (Figure 2b). In the case of AM/CNF/PLA films, peaks were observed around 7.6°, 12.6°, 17.4°, 20°, and 22.3° (Figure 2c). The peak around 22.3° indicated the presence of the crystalline type-I structure of CNF. Similarly, the WAXS pattern of the AM/g-CNF/PLA films exhibited peaks consistent with those of AM/CNF/PLA films, with higher intensities observed at 17.4° due to the higher PLA content (Figure 2d).
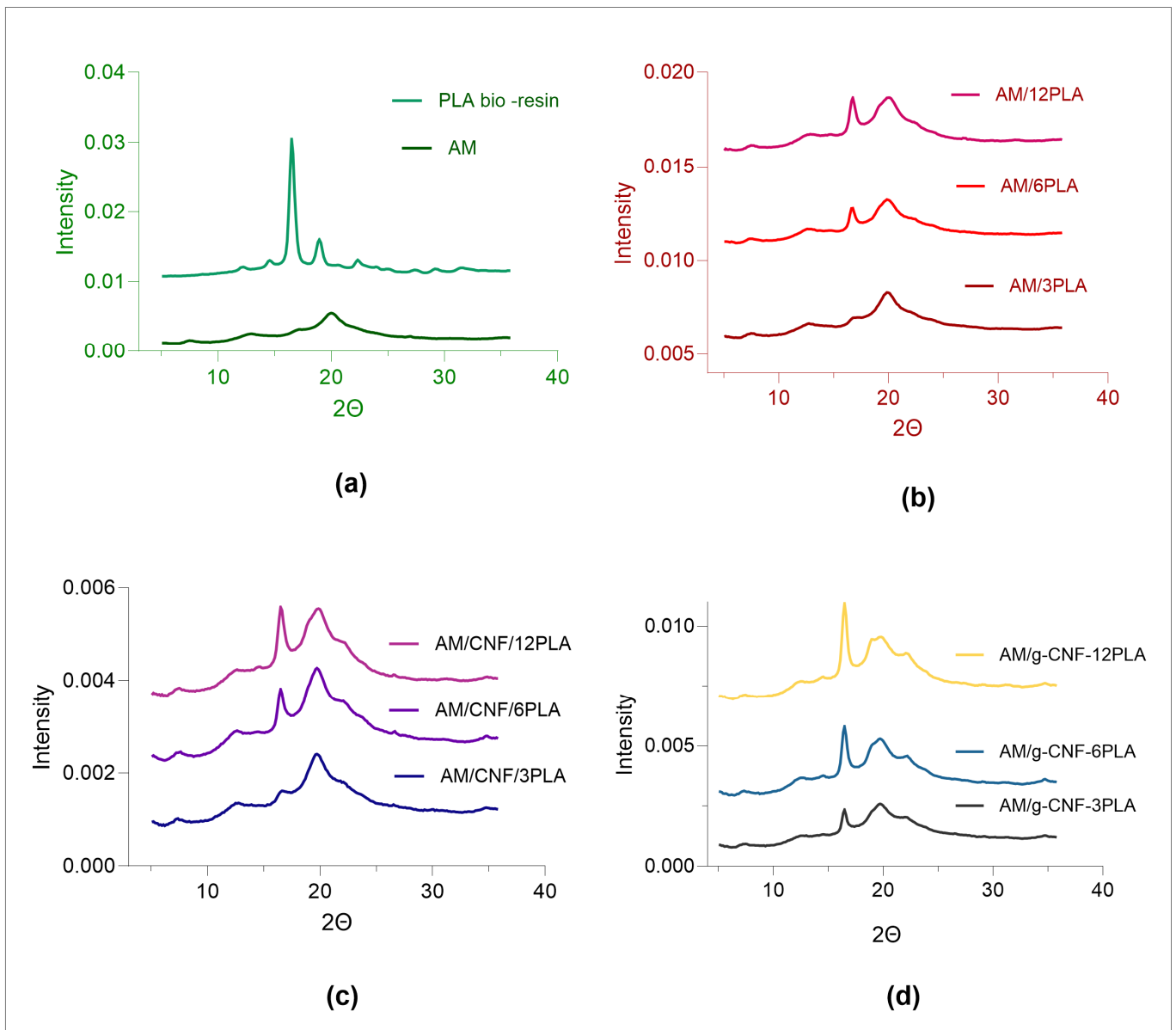
Figure 2. WAXS of (**a**) AM film and WAXS of composite films of (**b**) AM/PLA, (**c**) M/CNF-PLA, (**d**) AM/g-CNF-PLA.

3.4. Moisture Content

The AM/PLA films exhibited a significant reduction in moisture content (MC) after the addition of PLA, which is attributed to its hydrophobic nature, compared to the AM control. However, the 6PLA film showed a relatively insignificant reduction in MC compared to the control, with a mean value of 20%. Upon the addition of CNF, noticeable fluctuations in the MC values were observed. Specifically, the AM/CNF/6PLAfilm exhibited the highest MC, with a mean value of 23%, albeit generally lower than that of the AM/PLA films. The pattern observed in AM/g-CNF/PLA films was similar to that of AM/PLA, with the exception of a lower MC. Notably, the AM/g-CNF/PLA films demonstrated the lowest MC among the grafted CNF samples, with a value of 12% (Figure 3a).
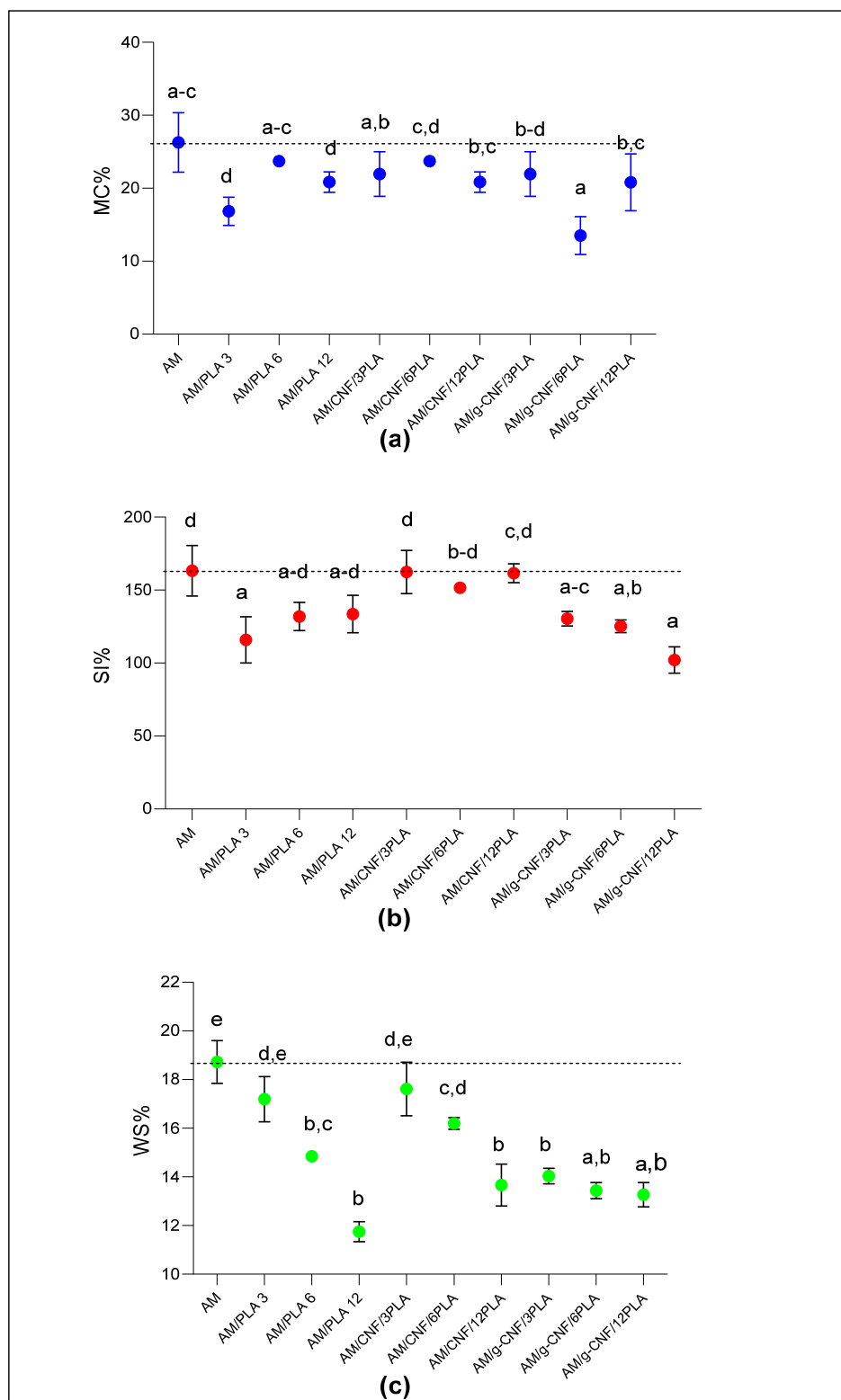
Figure 3. Physical properties of the composite films: (**a**) moisture content (MC %), (**b**) swelling index (SI %), (**c**) water solubility (WS %). Different letters represent statistical differences ($p \leq 0.05$).

3.5. Swelling Index and Water Solubility

Swelling index (SI) is a measure of water absorption and thus depends on hydrophilicity and the water-accessible pore volume. A significant difference was observed with increasing concentrations of PLA (Figure 3b). However, no change in the SI was observed

in the AM/CNF/PLA composites. However, the AM/g-CNF/PLA films showed a significant decrease in SI compared to AM, with the AM/g-CNF/12PLA film exhibiting the lowest mean SI of 102%. This suggests high compatibility between AM and PLA after the addition of g-CNF.

WS is a measure of loss of mass following a hydration–dehydration cycle. The incorporation of PLA led to a significant decrease in WS as the PLA percentage increased for both AM/PLA and AM/CNF/PLA films (Figure 3c). The WS of the AM/g-CNF/PLA films was lower compared to the non-grafted CNF films. However, the 12% PLA film stood out with the lowest mean WS value of 12%. This indicates that the addition of PLA can reduce the solubility of the composite bioplastic and improve its water barrier properties, which is consistent with the results of the contact angle measurement [15].

3.6. Mechanical Properties

The mechanical properties of AM/PLA composites are summarized in Table 2. Blending AM with PLA decreased the tensile strength proportionally with the content of PLA due to poor compatibility between starch and PLA. On the other hand, the elongation at break (EAB) of AM/PLA composites decreased with increasing PLA. Adding PLA can raise tensile strength and decrease the EAB. PLA is brittle and has a high tensile strength (55.4 MPa) and low EAB (<10%), and is known to affect the tensile properties of bioplastic composites prepared using hot pressing or extrusion at a higher pressure and temperature [15,39]. The Pickering emulsion approach aims to stabilize polar and hydrophobic phases containing a polymer within an aqueous medium containing hydrophilic cellulose. There was a significant difference in the tensile strength values of AM/CNF/3PLA and AM/CNF/6PLA, which were 21.3 and 17.1 MPa, respectively.

Table 2. Mechanical properties of AM/PLA blends, AM/CNF/PLA and AM/g−CNF/PLA. Different letters represent statistical differences ($p \leq 0.05$).

Code	Tensile Strength (MPa)	EAB (%)	Relative Crystallinity (%)
AM	11.4 ± 0.4 [b]	28.2 ± 1.7 [e]	21.9 ± 0.1 [a]
AM/PLA 3	7.7 ± 3.5 [a,b]	19.0 ± 5.2 [c,d]	24 ± 1.4 [a,b]
AM/PLA 6	5.9 ± 0.1 [a,b]	16.6 ± 4.5 [d]	29.5 ± 2.9 [a,b]
AM/PLA 12	3.5 ± 0.4 [a]	8.9 ± 1.0 [b,c]	31.2 ± 3.7 [a,b]
AM/CNF/3PLA	21.3 ± 2.3 [c]	3.0 ± 1.3 [a,b]	32.6 ± 1.8 [a,b]
AM/CNF/6PLA	17.1 ± 2.6 [c]	8.7 ± 3.9 [b,c]	34.5 ± 1.5 [a,b]
AM/CNF/12PLA	2.8 ± 0.5 [a]	1.1 ± 0.2 [a]	38 ± 4.0 [a]
AM/g-CNF/3PLA	18.4 ± 4.8 [c]	6.0 ± 2.9 [a,b]	33.5 ± 0.7 [a,b]
AM/g-CNF/6PLA	20.2 ± 4.6 [c]	4.5 ± 1.9 [a,b]	32.6 ± 1.9 [a,b]
AM/g-CNF/12PLA	8.8 ± 4.5 [a,b]	4.4 ± 2.0 [a,b]	37.1 ± 3 [a,b]

However, by increasing the content of PLA to 12%, the strength decreased to 2.8 MPa due to the nature of the composite matrices, which lead to inhomogeneity and incompatibility with the blend, resulting in phase separation [34,40]. Fiber can effectively reinforce a softer matrix, such as an AM/PLA blend, more than a rigid PLA matrix, resulting in lower impact strength for the AM/PLA/CNF composite. This can be related to the SEM imaging of AM/CNF/12PLA with some ragged and void structure that caused brittle fractures (Figure 4). The same trend was observed with AM/g-CNF/PLA composite samples.
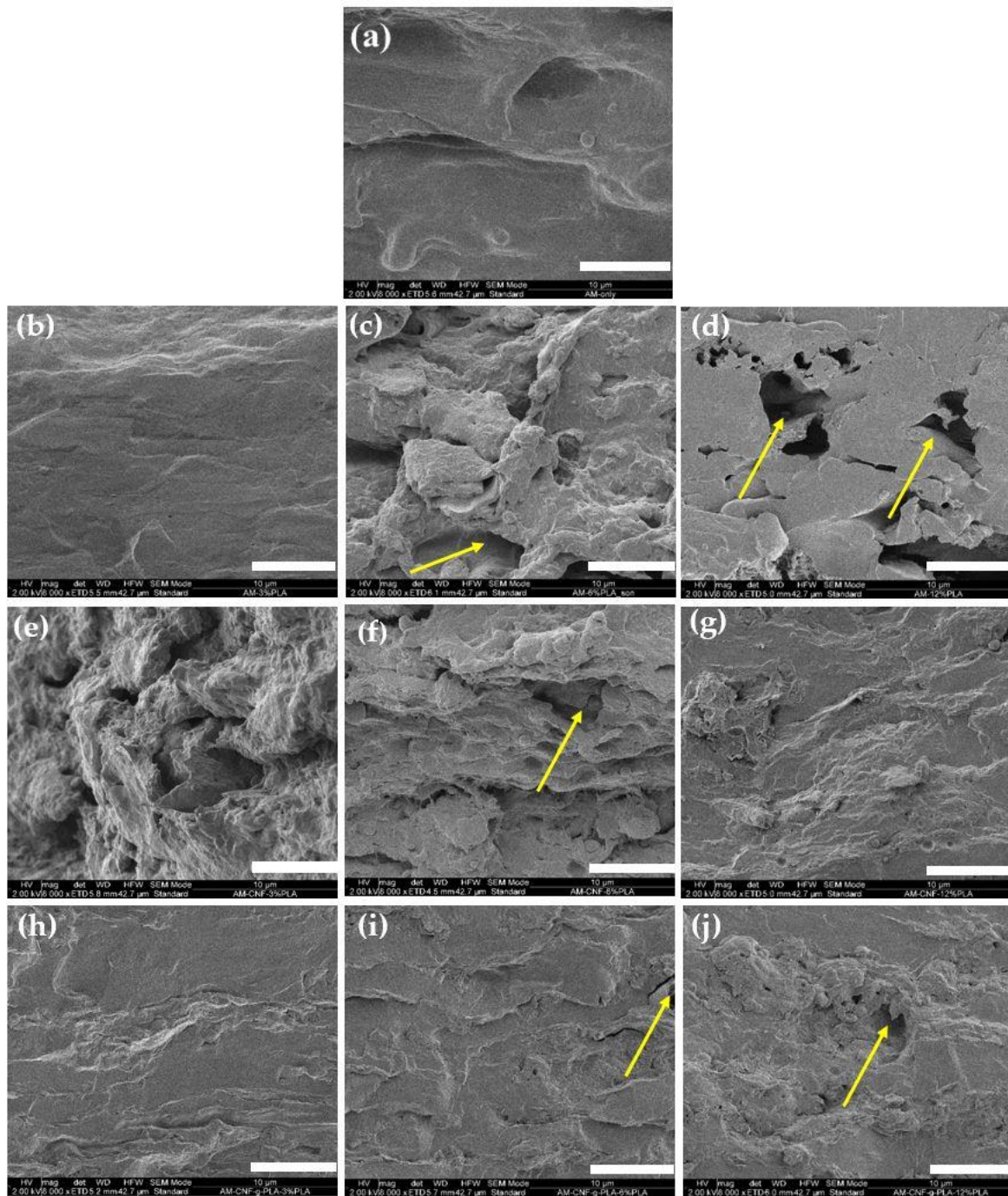
Figure 4. SEM images of the cross-section of; (**a**) AM film, (**b–d**) AM/PLA composite film, (**e–g**) AM/CNF/PLA, and (**h–j**) AM/g-CNC/PLA composite film. Arrows point to voids. Scale bar, 10 μm.

3.7. SEM

The cross-section images of the blend films (Figure 4) revealed notable differences in the inner structure of the different composite films. The AM film exhibited a homogeneous cross-sectional surface, suggesting a uniform distribution of starch particles. The introduction of glycerol appeared to prevent the aggregation of starch particles, as glycerol remained and solvated between the starch polymeric chains (Figure 4a), resulting in minimal agglomerations between the polymers. Upon comparing the cross-sections, the 3%

PLA film appeared uniform and smooth, whereas an increase in PLA content led to the presence of large voids and indents, indicating prominent phase separation.

The cross-sections of the AM/PLA/CNF (Figure 4e–g) appeared considerably more homogeneous compared to the AM/PLA films, exhibiting no phase separation but rather a rugged structure. The increasing concentration of PLA appeared to alter the surface and cross-section morphology. In the AM/g-CNF/PLA samples (Figure 4h–j), agglomerations of what are most likely CNF fibers were observed, with the tendency for agglomerations to increase with higher PLA content. The morphology otherwise showed successful homogenization in the AM/g-CNF/3PLA system, but became inconsistent in the AM/g-CNF/12PLA samples, with small indents starting to appear in the cross-sections, resulting in poor interfacial adhesion between PLA and AM.

Film appearance and the SEM surface morphology analysis of all the films (Figures S3 and S4) indicated that the g-CNF systems appeared to form dry films and detached from the composite AM/PLA matrix because of a fracture mechanism. For particulate-filled composites containing a coupling agent [22], wetting and bonding at the interface significantly affect the properties of the composite. The first step in forming an adhesive bond requires interfacial molecular contact by wetting. Molecules diffuse across the interface and react chemically to form covalent bonds. In a well-wetted blend, there are few voids and trapped air bubbles in the dry samples due to the reduced surface tension of the matrix (Figure S3).

PLA has a melting temperature of about 170–190 °C, which is higher than the drying temperature used in our study. The interfacial adhesion might be increased via pressing at higher temperatures or using a lower content of g-CNF to avoid agglomeration. These results suggest that adding lower content of 6% PLA is optimal for both binary and ternary blends with AM.

3.8. Wettability by Water Contact Angle

The water contact angle provides a measure for the surface capacity to adsorb water. Wettability refers to the valuation of contact angles, which indicates the extent of wetting between a liquid and a solid surface. Hydrophilic surfaces are regarded having a contact angle $< 90°$, while hydrophobic surfaces $\geq 90°$. The PLA contact angle is 110.10° [41], classifying it as considerably more hydrophobic than AM with a contact angle of 70° (Figure 5).
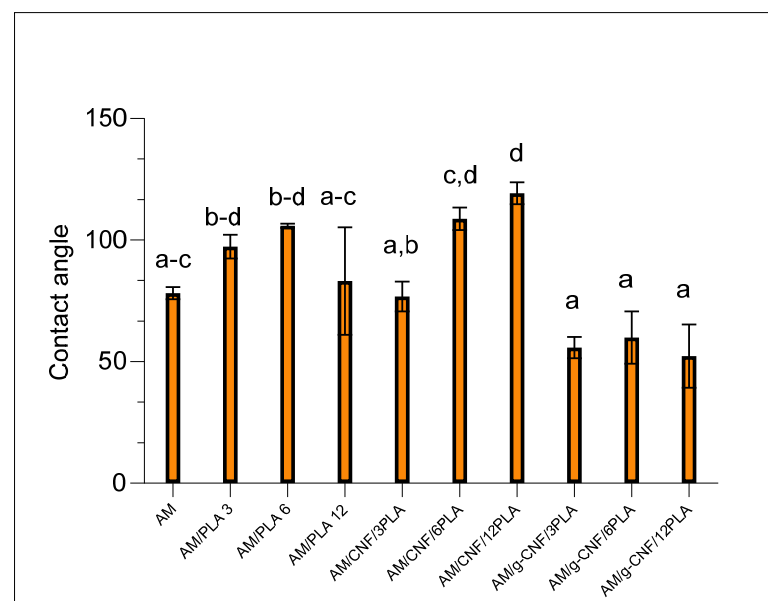
Figure 5. Average CA of blended composite films. Different letters represent statistical differences ($p \leq 0.05$).

The wettability analysis of the composite polymeric films achieved by using the sessile drop method (Figure 5) revealed the hydrophilic nature of AM (contact angle < 90°), which decreased in AM/PLA composites and AM/CNF/PLA (CA > 90°), demonstrating the hydrophobic characteristics of PLA and that it significantly possessed higher wettability with composite AM/CNF/12PLA compared to AM as a control. For the AM/g-CNF/PLA composites, inclined results were observed. It was expected that the presence of g-CNF could increase the water repulsion; however, it was lower (contact angle < 90°) with no significant differences between the composites, and this might be due to the aggregation of g-CNF, resulting in phase separation between the AM and PLA matrices.

4. Conclusions

A number of studies have demonstrated the feasibility of using PLA as a composite component in starch composite blends. Our study focuses on utilizing bulk-produced AM combined with PLA and g-CNF systems using Pickering emulsion fabrication protocols to enhance the polymer compatibility and tensile strength of the composites. SEM micrographs revealed homogeneous cross-sections and surfaces at low PLA content. However, at 25% of g-CNF, PLA exhibited a weak interaction with AM, which was overcome through reducing the PLA content due to the agglomeration of g-CNF. The addition of CNF and g-CNF enhanced the tensile strength and crystallinity of the composite blends due to the compatibility between AM and CNF. Composites with g-CNF showed lower wettability, water solubility and a higher swelling index. For future studies, the compounding of AM/PLA matrices should be evaluated at higher temperatures to allow molecular diffusion and mobility, thereby reducing the interfacial adhesion between the hydrophobic nature of PLA and polysaccharides.

References

1. Thompson, R.C.; Moore, C.J.; Saal, F.S.V.; Swan, S.H. Plastics, the Environment and Human Health: Current Consensus and Future Trends. *Philos. Trans. R. Soc. B Biol. Sci.* **2009**, *364*, 2153–2166. [CrossRef] [PubMed]

2.   Moshood, T.D.; Nawanir, G.; Mahmud, F.; Mohamad, F.; Ahmad, M.H.; AbdulGhani, A. Sustainability of Biodegradable Plastics: New Problem or Solution to Solve the Global Plastic Pollution? *Curr. Res. Green Sustain. Chem.* **2022**, *5*, 100273. [CrossRef]

3.   Faisal, M.; Kou, T.; Zhong, Y.; Blennow, A. High Amylose-Based Bio Composites: Structures, Functions and Applications. *Polymers* **2022**, *14*, 1235. [CrossRef] [PubMed]

4.   Zhong, Y.; Tai, L.; Blennow, A.; Ding, L.; Herburger, K.; Qu, J.; Xin, A.; Guo, D.; Hebelstrup, K.H.; Liu, X. High-Amylose Starch: Structure, Functionality and Applications. *Crit. Rev. Food Sci. Nutr.* **2023**, *63*, 8568–8590. [CrossRef] [PubMed]

5.   Sagnelli, D.; Hebelstrup, K.H.; Leroy, E.; Rolland-Sabaté, A.; Guilois, S.; Kirkensgaard, J.J.K.; Mortensen, K.; Lourdin, D.; Blennow, A. Plant-Crafted Starches for Bioplastics Production. *Carbohydr. Polym.* **2016**, *152*, 398–408. [CrossRef] [PubMed]

6.   Carciofi, M.; Blennow, A.; Jensen, S.L.; Shaik, S.S.; Henriksen, A.; Buléon, A.; Holm, P.B.; Hebelstrup, K.H. Concerted Suppression of All Starch Branching Enzyme Genes in Barley Produces Amylose-Only Starch Granules. *BMC Plant Biol.* **2012**, *12*, 223. [CrossRef] [PubMed]

7.   Sagnelli, D.; Hooshmand, K.; Kemmer, G.C.; Kirkensgaard, J.J.K.; Mortensen, K.; Giosafatto, C.V.L.; Holse, M.; Hebelstrup, K.H.; Bao, J.; Stelte, W.; et al. Cross-Linked Amylose Bio-Plastic: A Transgenic-Based Compostable Plastic Alternative. *Int. J. Mol. Sci.* **2017**, *18*, 2075. [CrossRef] [PubMed]

8.   Luyt, A.S.; Malik, S.S. *Can Biodegradable Plastics Solve Plastic Solid Waste Accumulation?* Elsevier Inc.: Amsterdam, The Netherlands, 2018; ISBN 9780128131404.

9.   DeStefano, V.; Khan, S.; Tabada, A. Applications of PLA in Modern Medicine. *Eng. Regen.* **2020**, *1*, 76–87. [CrossRef] [PubMed]

10. Sharafi Zamir, S.; Fathi, B.; Ajji, A.; Robert, M.; Elkoun, S. Crystallinity and Gas Permeability of Poly (Lactic Acid)/Starch Nanocrystal Nanocomposite. *Polymers* **2022**, *14*, 2802. [CrossRef]

11. Pluta, M.; Jeszka, J.K.; Boiteux, G. Polylactide/Montmorillonite Nanocomposites: Structure, Dielectric, Viscoelastic and Thermal Properties. *Eur. Polym. J.* **2007**, *43*, 2819–2835. [CrossRef]

12. Wang, T.; Yang, Y.; Zhang, C.; Tang, Z.; Na, H.; Zhu, J. Effect of 1,3,5-Trialkyl-Benzenetricarboxylamide on the Crystallization of Poly(Lactic Acid). *J. Appl. Polym. Sci.* **2013**, *130*, 1328–1336. [CrossRef]

13. Fonseca-García, A.; Osorio, B.H.; Aguirre-Loredo, R.Y.; Calambas, H.L.; Caicedo, C. Miscibility Study of Thermoplastic Starch/Polylactic Acid Blends: Thermal and Superficial Properties. *Carbohydr. Polym.* **2022**, *293*, 119744. [CrossRef] [PubMed]

14. Martinez Villadiego, K.; Arias Tapia, M.J.; Useche, J.; Escobar Macías, D. Thermoplastic Starch (TPS)/Polylactic Acid (PLA) Blending Methodologies: A Review. *J. Polym. Environ.* **2022**, *30*, 75–91. [CrossRef]

15. Abdullah, A.H.D.; Fikriyyah, A.K.; Putri, O.D.; Puspa Asri, P.P. Fabrication and Characterization of Poly Lactic Acid (PLA)-Starch Based Bioplastic Composites. *IOP Conf. Ser. Mater. Sci. Eng.* **2019**, *553*, 012052. [CrossRef]

16. Wokadala, O.C.; Emmambux, N.M.; Ray, S.S. Inducing PLA/Starch Compatibility through Butyl-Etherification of Waxy and High Amylose Starch. *Carbohydr. Polym.* **2014**, *112*, 216–224. [CrossRef] [PubMed]

17. Chauhan, S.; Raghu, N.; Raj, A. Effect of Maleic Anhydride Grafted Polylactic Acid Concentration on Mechanical and Thermal Properties of Thermoplasticized Starch Filled Polylactic Acid Blends. *Polym. Polym. Compos.* **2021**, *29*, S400–S410. [CrossRef]

18. Clasen, S.H.; Müller, C.M.O.; Pires, A.T.N. Maleic Anhydride as a Compatibilizer and Plasticizer in TPS/PLA Blends. *J. Braz. Chem. Soc.* **2015**, *26*, 1583–1590. [CrossRef]

19. Akrami, M.; Ghasemi, I.; Azizi, H.; Karrabi, M.; Seyedabadi, M. A New Approach in Compatibilization of the Poly(Lactic Acid)/Thermoplastic Starch (PLA/TPS) Blends. *Carbohydr. Polym.* **2016**, *144*, 254–262. [CrossRef]

20. Xu, J.; Sagnelli, D.; Faisal, M.; Perzon, A.; Taresco, V.; Mais, M.; Giosafatto, C.V.L.; Hebelstrup, K.H.; Ulvskov, P.; Jørgensen, B.; et al. Amylose/Cellulose Nanofiber Composites for All-Natural, Fully Biodegradable and Flexible Bioplastics. *Carbohydr. Polym.* **2021**, *253*, 117277. [CrossRef]

21. Perzon, A.; Jørgensen, B.; Ulvskov, P. Sustainable Production of Cellulose Nanofiber Gels and Paper from Sugar Beet Waste Using Enzymatic Pre-Treatment. *Carbohydr. Polym.* **2020**, *230*, 115581. [CrossRef]

22. Goffin, A.L.; Raquez, J.M.; Duquesne, E.; Siqueira, G.; Habibi, Y.; Dufresne, A.; Dubois, P. From Interfacial Ring-Opening Polymerization to Melt Processing of Cellulose Nanowhisker-Filled Polylactide-Based Nanocomposites. *Biomacromolecules* **2011**, *12*, 2456–2465. [CrossRef] [PubMed]

23. Fang, L.; Qi, R.; Liu, L.; Juan, G.; Huang, S. Synthesis of Poly(L-Lactide) via Solvothermal Method. *Int. J. Polym. Sci.* **2009**, *2009*, 929732. [CrossRef]

24. Lee, S.; Kim, C.H.; Park, J.K. Improvement of Processability of Clay/Polylactide Nanocomposites by a Combinational Method: In Situ Polymerization of L-Lactide and Melt Compounding of Polylactide. *J. Appl. Polym. Sci.* **2006**, *101*, 1664–1669. [CrossRef]

25. Wu, H.; Nagarajan, S.; Zhou, L.; Duan, Y.; Zhang, J. Synthesis and Characterization of Cellulose Nanocrystal-Graft-Poly(D-Lactide) and Its Nanocomposite with Poly(L-Lactide). *Polymer* **2016**, *103*, 365–375. [CrossRef]

26. Gauss, C.; Pickering, K.L. A New Method for Producing Polylactic Acid Biocomposites for 3D Printing with Improved Tensile and Thermo-Mechanical Performance Using Grafted Nanofibrillated Cellulose. *Addit. Manuf.* **2023**, *61*, 103346. [CrossRef]

27. Li, L.; Chen, Y.; Yu, T.; Wang, N.; Wang, C.; Wang, H. Preparation of Polylactic Acid/TEMPO-Oxidized Bacterial Cellulose Nanocomposites for 3D Printing via Pickering Emulsion Approach. *Compos. Commun.* **2019**, *16*, 162–167. [CrossRef]

28. Abdulkhani, A.; Hosseinzadeh, J.; Ashori, A.; Dadashi, S.; Takzare, Z. Preparation and Characterization of Modified Cellulose Nanofibers Reinforced Polylactic Acid Nanocomposite. *Polym. Test.* **2014**, *35*, 73–79. [CrossRef]

29. Ansari, F.; Skrifvars, M.; Berglund, L. Nanostructured Biocomposites Based on Unsaturated Polyester Resin and a Cellulose Nanofiber Network. *Compos. Sci. Technol.* **2015**, *117*, 298–306. [CrossRef]

30. Bataille, P.; Statioukha, G.; Statioukha, O. Simulation and Optimization of Cellulose and Styrene Graft Copolymerization Process. *Can. J. Chem. Eng.* **1996**, *74*, 501–510. [CrossRef]

31. Faisal, M.; Žmirić, M.; Kim, N.; Bruun, S.; Mariniello, L.; Famiglietti, M.; Bordallo, H.; Kirkensgaard, J.; Jørgensen, B.; Ulvskov, P.; et al. A Comparison of Cellulose Nanocrystals and Nanofibers as Reinforcements to Amylose-Based Composite Bioplastics. *Coatings* **2023**, *13*, 1573. [CrossRef]

32. Gontard, N.; Duchez, C.; Cuq, J.-L.; Guilbert, S. Edible Composite Films of Wheat Gluten and Lipids: Water Vapour Permeability and Other Physical Properties. *Int. J. Food Sci. Technol.* **1994**, *29*, 39–50. [CrossRef]

33. Chisenga, S.M.; Workneh, T.S.; Bultosa, G.; Laing, M. Characterization of Physicochemical Properties of Starches from Improved Cassava Varieties Grown in Zambia. *AIMS Agric. Food* **2019**, *4*, 939–966.

34. Yoksan, R.; Boontanimitr, A.; Klompong, N. Poly (Lactic Acid)/Thermoplastic Cassava Starch Blends Filled with Duckweed Biomass. *Int. J. Biol. Macromol.* **2022**, *203*, 369–378. [CrossRef] [PubMed]

35. Miao, C.; Hamad, W.Y. In-Situ Polymerized Cellulose Nanocrystals (CNC)—Poly(L-Lactide) (PLLA) Nanomaterials and Applications in Nanocomposite Processing. *Carbohydr. Polym.* **2016**, *153*, 549–558. [CrossRef] [PubMed]

36. Rammak, T.; Boonsuk, P.; Kaewtatip, K. Mechanical and Barrier Properties of Starch Blend Films Enhanced with Kaolin for Application in Food Packaging. *Int. J. Biol. Macromol.* **2021**, *192*, 1013–1020. [CrossRef] [PubMed]

37. Vaezi, K.; Asadpour, G.; Sharifi, H. Effect of ZnO Nanoparticles on the Mechanical, Barrier and Optical Properties of Thermoplastic Cationic Starch/Montmorillonite Biodegradable Films. *Int. J. Biol. Macromol.* **2019**, *124*, 519–529. [CrossRef]

38. Cuevas-Carballo, Z.B.; Duarte-Aranda, S.; Canché-Escamilla, G. Properties and Biodegradation of Thermoplastic Starch Obtained from Grafted Starches with Poly(Lactic Acid). *J. Polym. Environ.* **2019**, *27*, 2607–2617. [CrossRef]

39. Nazrin, A.; Sapuan, S.M.; Zuhri, M.Y.M. Mechanical, Physical and Thermal Properties of Sugar Palm Nanocellulose Reinforced Thermoplastic Starch (TPS)/Poly (Lactic Acid) (PLA) Blend Bionanocomposites. *Polymers* **2020**, *12*, 2216. [CrossRef] [PubMed]

40. Chotiprayon, P.; Chaisawad, B.; Yoksan, R. Thermoplastic Cassava Starch/Poly(Lactic Acid) Blend Reinforced with Coir Fibres. *Int. J. Biol. Macromol.* **2020**, *156*, 960–968. [CrossRef]

41. Mohd Nizar, M.; Hamzah, M.S.A.; Abd Razak, S.I.; Mat Nayan, N.H. Thermal Stability and Surface Wettability Studies of Polylactic Acid/Halloysite Nanotube Nanocomposite Scaffold for Tissue Engineering Studies. *IOP Conf. Ser. Mater. Sci. Eng.* **2018**, *318*, 012006. [CrossRef]